Internal structure and emplacement mechanism of composite plutons: Evidence from Mt Kinabalu, Borneo

Alex Burton-Johnson*[1]; Colin G. Macpherson[2] & Robert Hall[3]

[1]British Antarctic Survey, High Cross, Madingley Road, Cambridge, CB3 0ET, UK

*Corresponding author (e-mail: alerto@bas.ac.uk)

[2]Department of Earth Sciences, University of Durham, Durham, DH1 3LE, UK

[3]SE Asia Research Group, Department of Geology, Royal Holloway, University of London, Egham, Surrey TW20 0EX, UK

Word count

Abstract and body: 5,649

Table and figure captions: 757

References: 1,790

Number of Figures

12

Keywords

Mt Kinabalu, SE Asia, emplacement, tectonics, intrusion, pluton, granite, granodiorite

Abstract

The internal structure and emplacement mechanisms of composite plutons are investigated using new field data from the composite Late Miocene granitic intrusion of Mt Kinabalu in northern Borneo. The pluton was emplaced in the upper to middle crust in the Late Miocene at the contact between the ultramafic basement and sedimentary cover rocks. Structural data indicates that emplacement occurred during regional NNW-SSE oriented extension, challenging tectonic models that infer contemporaneous regional compression. The six major units comprising the pluton were accommodated by upward flexure of the cover rocks with most magma pulses emplaced successively beneath their predecessors. However, the irregular three-dimensional internal structure of the pluton also reflects preferential emplacement of successive units along the granite-country rock contact of previous units in preference to the basement-cover rock contact exploited by the initial units. This work highlights the complex emplacement mechanisms and internal structure of composite intrusions and assesses how they differ from models of tabular emplacement.

Introduction

Interpretations of ascent and emplacement of granitic intrusions have changed drastically in recent decades from models of large diapirs ascending slowly through the crust to models of rapid dyke-fed ascent and layered, laccolith-style emplacement of composite plutons (Clemens & Mawer 1992, Petford *et al.* 2000, Petford & Clemens 2000, McCaffrey & Petford 1997, Cruden 1998, Cruden & McCaffrey 2001, Grocott *et al.* 2009, Vigneresse & Clemens 2000, Horsman *et al.* 2009, de Silva & Gosnold 2007, de Saint-Blanquat *et al.* 2001, de Saint-Blanquat *et al.* 2006, Vigneresse 2006, Wiebe & Collins 1998, Wiebe 1988). Mt Kinabalu in Sabah, NW Borneo (Fig. 1), is an Upper Miocene intrusion with a 4095 m high glaciated summit and good exposure over a vertical range of 2900m (Fig. 2), providing an excellent opportunity to study the structure of a granitoid pluton in three dimensions. Cottam *et al.* (2010) reinterpreted the intrusion as a composite laccolith formed by discrete magmatic pulses based on geochronological constraints. However, no detailed mapping of the pluton has been undertaken for four decades, largely due to its extreme relief and difficulties in accessing its densely forested flanks. We present the first new map of the pluton since Jacobson (1970) and reinterpret its structure and emplacement, then discuss the implications for global magmatic processes.

Regional geological history and tectonic setting

Northern Borneo has a basement of Mesozoic igneous and metamorphic rocks overlain by Cenozoic sediments. The basement includes mafic igneous rocks and radiolarian cherts, variably serpentinised peridotites and Triassic to Cretaceous rocks previously described as crystalline basement (Reinhard & Wenk 1951, Dhonau & Hutchison 1965, Koopmans 1967, Kirk 1968, Leong 1974). The latter resemble deformed ophiolitic rocks intruded by arc plutonic rocks that Hall & Wilson (2000) suggested formed in a Mesozoic, intra-oceanic arc. The peridotites have been interpreted as part of a Cretaceous ophiolite (Hutchison 2005) emplaced in the Late Cretaceous or Early Paleogene (Newton-Smith 1967, Omang & Barber 1996). Unusual peridotites exposed close to Mount Kinabalu have been interpreted to represent sub-continental mantle (Imai & Ozawa 1991). The basement is in contact with a cover sequence of predominantly deep-water turbidites

and related deposits assigned to the Eocene to Lower Miocene Trusmadi and Crocker Formations (Collenette 1965, van Hattum *et al.* 2006).

The basement and cover rocks were folded and faulted during Eocene and Oligocene deformation that was driven by the subduction of the proto-South China Sea beneath Borneo (Taylor & Hayes 1983; Rangin & Silver 1990; Tongkul 1991, 1994; Hall 1996; Hall & Wilson 2000; Hutchison 2000). The attenuated South China continental margin collided with northern Borneo in the Early Miocene (Hutchison 2000, Hall & Wilson 2000) resulting in the Sabah Orogeny (Hutchison 1996), which produced significant topography in the region (Hutchison 2000) and emergence of much of Sabah and the present central highlands of northern Borneo. However, by the end of the Early Miocene much of present-day Sabah was below or close to sea level (Noad 1998, Balaguru *et al.* 2003, Hall *et al.* 2008), probably with a low elevated range of hills at the position of the Crocker Mountains. Offshore the Neogene shelf edge migrated broadly northwestwards from the Middle Miocene onwards (Sandal 1996, Hazebroek & Tan 1993, Hutchison 2005, Cullen 2010), suggesting a gradual rise and widening of the Crocker Mountains during the Middle and Late Miocene. The Kinabalu granite was intruded into the centre of the Crocker Mountains between 8 and 7 Ma (Cottam *et al.* 2010). High post-emplacement exhumation rates indicated by low temperature thermochronology are comparable to the exhumation rates of mountainous terrains (Cottam *et al.* 2013), suggesting that the Crocker Range existed at the time of emplacement.

Sabah became fully emergent only at the end of the Miocene or Early Pliocene (Collenette 1965, Balaguru *et al.* 2003, Tongkul & Chang 2003, Morley & Back 2008). The glaciated summit plateaus and Pleistocene glacial tills (Collenette 1958) of the Kinabalu area, and similar deposits near to Mount Tambuyukon, indicate that the summits of Kinabalu, Tambuyukon and possibly Trusmadi, were significantly higher than other parts of the Crocker Range by the Pleistocene.

Results

New geological maps

A limited number of field studies on the geology of Mt Kinabalu have been published (Reinhard & Wenk 1951, Collenette 1958, Kasama *et al.* 1970, Jacobson 1970). At the time of this previous mapping the mountain was even less accessible than today with more extensive rainforest cover and much poorer transport systems. As such, access was largely restricted to the lowland streams south of the mountain. Our work augments the observations of Jacobson (1970), the most recent detailed study, with new traverses of the intrusion focusing on the previously unmapped high altitude regions including the eastern and northern ridges.

A new digital elevation model (DEM) was created during this study based on published topographic maps, a high resolution satellite image (1m resolution) and GPS observations collected during fieldwork. Fig. 3 presents the revised geological map of Mt. Kinabalu. Draping the map over the digital elevation model in Fig. 4 illustrates how the relief is controlled by the surface lithologies. Localities referred to on the summit plateaux are highlighted on the large scale summit map in Fig. 5. Combining the field observations with the chronology of Cottam *et al.* (2010) allows us to infer the internal structure of the pluton (Figs. 6 and 7).

Lithological Units

Ophiolitic basement

The ophiolitic basement is the oldest lithological unit in Sabah and underlies much of the region (Fig. 1). Outcrops of the ophiolite around Mt Kinabalu are predominantly lherzolite but there is also wehrlite, harzburgite and dunite, with varying degrees of serpentinisation (Jacobson 1970).

Fluvial pebbles 11km SE of Mt Kinabalu comprise garnet pyroxenites (in agreement with Imai & Ozawa 1991), amphibolite, garnet amphibolite, garnet-zeolite amphibolite and amphibolite-plagioclase gneiss, amygdale-rich basaltic volcanics and chert. Some of these lithologies are similar to rocks described from the Darvel Bay ophiolite (Leong

1974, Hutchison 1978, Omang & Barber 1996) and also resemble the description of Mt Kinabalu's "crystalline basement" (Jacobson 1970).

Ultramafic hornfels containing relict olivine and orthopyroxene with secondary chlorite, serpentine and talc is found downstream of the granite-ophiolite contact on the SE of the pluton in the river of S. Bambangan (Fig. 3). Some of the ultramafic rocks in contact with the Paka Porphyritic Granite on the summit trail are variably (sometimes intensively) altered to talc, and schists containing varying abundances of tremolite, anthophyllite and talc are described on the south of the mountain by Jacobson (1970).

Crocker Formation turbidite sediments

The interbedded turbiditic mudstones and quartzarenite to subarkose sandstones of the Crocker Formation overlie the ophiolitic basement. The contact was not observed on the north of the mountain but a metamorphic aureole of sandstones metamorphosed to quartzite extends ~20m to 2 km from the pluton. The contact between the sediments and granite was observed in S. Tahobang to the west of the intrusion (Fig. 3). For up to 8 m from the contact, sedimentary rocks have been metamorphosed to a hornfels of very fine sutured quartz grains, chlorite, minor biotite, and interstitial secondary muscovite. Jacobson (1970) observed contact metamorphism up to 1.6 km from the pluton where a mica-cordierite hornfels close to the contact in S. Kilambuan (west of the mountain, Fig. 3) contains biotite, muscovite, cordierite quartz and albite.

The Mt Kinabalu Pluton

The Mt Kinabalu pluton comprises six major units classified by modal mineral abundances determined by point counting of 46 thin sections stained for plagioclase and K-Feldspar (Sperber 2009). Table 1 presents the modal mineralogy of these intrusive units, along with U-Pb ages from zircon rims (Cottam *et al.*, 2010). Estimates of volumes for each unit are included based on the mapped extent (Fig. 3) and the interpreted pre-erosion cross-section of the pluton (Fig. 6). Calculation of these volumes is discussed further in the 'Discussion' section below. Although the modal mineralogy of many of the units are very similar, they can be distinguished in the field (although sometimes only on fresh surfaces) and were mapped according to these mineralogical differences (with the

exception of the Low's Granite which was distinguished from the King Granite using mineralogical, chemical and magnetic susceptibility data).

Petrographic descriptions and field relationships between the units are given below, with more detailed information in Burton-Johnson (2013). We include two newly recognised units, the King Granite and the Paka Porphyritic Granite. The King Granite was previously mapped as part of the Low's Granite (under the name "Hornblende Granite", Cottam *et al.* 2010) and the Paka Porphyritic Granite was included as part of the Mesilau Porphyritic Granite (previously named the "Porphyritic Hornblende Granite", Cottam *et al.* 2010). The revised classification (Fig. 8) differs from previous work (Reinhard & Wenk 1951, Kirk 1968, Vogt & Flower 1989) as summarised in Cottam et al. (2010), which partly reflects changing classification schemes, and partly the result of mineral misidentifications in some earlier studies probably due to a lack of thin section mineral staining. Key differences are: (i) that we find more consistent modal mineralogies for each unit in this study than previous mineralogical data suggested; (ii) the Alexandra Tonalite/Granodiorite unit, previously classified as a monzodiorite (Vogt & Flower 1989), ranges from tonalite to granodiorite with varying potassium feldspar content (4-7%); and (iii) that the majority of units are granites, not granodiorites or quartz monzonites.

Alexandra Tonalite/Granodiorite

The Alexandra Tonalite/Granodiorite is the oldest unit and forms most of the western summit peaks of the Western Plateau. It is composed of 1-3 mm grains of quartz, plagioclase, K-feldspar, hornblende and biotite crystals. Biotite is the dominant ferromagnesian phase, although biotite pseudomorphs of hornblende indicate that much may be secondary. Secondary biotite occurs in all the granite units but is particularly prevalent in the Alexandra Tonalite/Granodiorite. Foliation of the biotite crystals was observed to dip at ~40-65° towards the south-west.

Low's Granite

The Low's Granite was emplaced below and around the Alexandra Tonalite/Granodiorite, forming the eastern and southern peaks on the Western Plateau and a separate unconnected region on the mountain's northern flank (Fig. 3). The unit is composed of 4-7 mm long euhedral prismatic hornblende phenocrysts (the dominant

ferromagnesian phase) in a groundmass of 1-4 mm grains of K-feldspar, plagioclase, hornblende and biotite. Samples from the northern flank contain more K-feldspar and quartz than those of the Western Plateau.

The contact of the Alexandra Tonalite/Granodiorite and Low's Granite was observed on the Western Plateau. Along the eastern extent of the Alexandra Tonalite/Granodiorite this contact steepens to vertical and in some places the Low's Granite is found above the Alexandra Tonalite/Granodiorite, enveloping the older unit (Fig. 7 and 9). West of this the contact dip shallows to ~20° to the WSW and becomes sub-parallel to the topographic surface, revealing windows of the Low's Granite within the Alexandra Tonalite/Granodiorite (Fig. 9). The contact is sharp when sub-vertical but appears to be more gradational (over 1-3 m) where dipping at a low angle. When sharp, the contact shows chlorite, hematite and epidote mineralisation along the contact surface and the Low's Granite shows a 2 m wide chilled margin of more intense irregular and contact-parallel fracturing, finer crystal sizes, more abundant biotite and extensive chlorite mineralisation of ferromagnesian minerals, grading in to its interior composition (Fig. 10a). No chilled margin is expressed in the Alexandra Tonalite/Granodiorite. These field relations support emplacement of the Low's Granite after the Alexandra Tonalite/Granodiorite.

King Granite

The most extensive unit is the King Granite, emplaced beneath the Low's Granite. Crystal sizes and mineralogy are similar to the Low's Granite but with a lower modal abundance of ferromagnesian phases (especially biotite) and a greater amount of K-feldspar. The contact can be observed on the eastern cliff of the Western Plateau (Fig. 10b). This inaccessible outcrop shows a lighter body of King Granite in sharp contact with the overlying, darker Low's Granite. The lighter body darkens gradationally away from the contact, which dips at ~50° NW. Dykes of King Granite with sharp contacts intrude the overlying Low's Granite (Fig. 10b) so the periphery of the Low's Granite had solidified during the 0.2 My time gap inferred from zircon geochronology (Cottam *et al.* 2010), and support emplacement of the King Granite after the Low's Granite. Elsewhere the Low's and King Granites are almost identical in the field so the contact location is largely

inferred from geochemical and Anisotropic Magnetic Susceptibility (AMS) data (Burton-Johnson 2013).

Donkey Granite

Jacobson (1970) described this unit as a minor biotite adamellite porphyry but our work shows it to be much more extensive than previously mapped, intruding the King Granite on the Western and Eastern Plateaux and in Low's Gully 600 m below (Fig. 5 and 10c). We interpret these three occurrences as a NE-trending, sub-vertical planar sheet, approximately 2.5 km long and 200 m wide. The Donkey Granite is mineralogically similar to the King Granite, composed of hornblende, biotite and ≤4 mm long subhedral tabular plagioclase phenocrysts in a finer hornblende, biotite, plagioclase, quartz and K-feldspar groundmass.

On the Western Plateau the sub-vertical western and eastern margins of the Donkey Granite are different from each other (Fig. 5). The eastern contact is largely gradational but becomes sharp where it forms the distinctive Donkey's Ears Peak (Fig. 10d). The western contact is sharp along its length with sub-vertical, contact-parallel flow banding within the Donkey Granite and localised magma mingling with the King Granite (Fig. 10e), implying that neither body was solid when the Donkey Granite was intruded.

Paka Porphyritic Granite

The Paka Porphyritic Granite was emplaced after the King Granite (based on contact relations and geochronology) along the southern flank of the pluton. It is found to the south and east of the Eastern Plateau and at lower elevations on the NW flank. The unit contains subhedral, tabular, K-feldspar megacrysts of 10-15 mm length in a groundmass of 2-5 mm long K-feldspar, plagioclase, quartz, hornblende and biotite crystals. Megacrysts commonly show long axis alignment plunging at a low angle (<26°) but with varying azimuths, even across a single outcrop.

The contact of the King and Paka Porphyritic Granites is sharp and often apparent in the topography as steep cliffs around the Eastern Plateau. Proximal to the King Granite, megacrysts become more abundant in the Paka Porphyritic Granite which also shows contact-parallel flow banding and megacryst alignment (Fig. 10f) implying emplacement

of the Paka Porphyritic Granite after the King Granite. Along Mt Kinabalu's southern flanks the contact dips steeply south (67-82° S) with the Paka Porphyritic Granite overlying the older unit, but the orientation changes on the Eastern Plateau where the Paka Porphyritic Granite underlies the King Granite (Fig. 6, 7 and 10g). Hydrothermal channelling proximal to the contact has produced strong haematite alteration of the overlying units, including at the consequently named "Red Rock Peak" on the Eastern Plateau (Fig. 5 and 10g).

Mesilau Porphyritic Granite

The southeast portion of the main pluton is composed of the Mesilau Porphyritic Granite, which also forms the mineralised satellite stock of the disused Mamut porphyry copper mine (Fig. 3). The northern extent of the main mass was not observed but is interpreted from prominent topographic ridges and valleys. Previously mapped as a variant of the Paka Porphyritic Granite, the Mesilau Porphyritic Granite shows clear differences in mineralogy, chemistry and field relations (Burton-Johnson 2013). Most notably the Mesilau Porphyritic Granite possesses large, 20-30 mm long, subhedral, tabular, K-feldspar megacrysts that comprise approximately 30% of the rock and are commonly aligned. The groundmass consists of 3-5 mm long crystals of K-feldspar, plagioclase, quartz, hornblende and biotite and ≤2% clinopyroxene.

We could not locate contacts of the Mesilau Porphyritic Granite with other units. These were inferred from changes in float on opposite sides of narrow streams and gullies to the south, where it is close to the Paka Porphyritic Granite, and the east, where it is adjacent to the King Granite.

Dykes

Pyroxene monzonite dykes form large ENE-WSW trending intrusions up to 20 m wide. On the west face of the mountain individual dykes can be traced for approximately 1 km vertically. Preferential erosion of the dykes is the cause of a number of large, linear depressions across the plateau and many of the gaps between the Diwali Pinnacles of the Western Plateau (Fig. 10h). These dykes contain porphyritic clinopyroxene and K-feldspar in a groundmass of quartz and feldspar. Some dykes were found with subhedral

to euhedral tabular K-feldspar phenocrysts ≤15 mm long oriented parallel to their margins.

Discussion

The new field evidence allows us to reinterpret the emplacement history and mechanisms of the Mount Kinabalu pluton and its internal structure. The data allows investigation of the pluton and individual unit volumes; the syn-magmatic tectonic setting; the magmatic emplacement mechanisms; and the individual units' spatial and temporal relationships. Based on this we consider the implications for magma emplacement processes.

Pluton thickness

Although the new geological map and contact geometry data allow interpretation of the three dimensional structure of the pluton (Fig. 6 and 7), the basal geometry is not exposed and an independent methodology must be used to assess our interpretations. Cruden & McCaffrey (2001) have proposed that a power law relates the thickness and length of laccoliths, plutons and batholiths:

$$T = 0.6(\pm 0.15)L^{0.6(\pm 0.1)} \qquad \text{[Equation 1]}$$

Importantly, Cruden & McCaffrey (2001) postulated that Equation 1 is consistent for all scales of pluton emplacement including individual bodies and large composite plutons. If this relationship is applicable to Mount Kinabalu then the 11.5 km equivalent circle diameter of the short (9 km) and long (15 km) axes predicts a pluton thickness of 2.6 km (±1.5 km). This thickness estimate implies that the intrusion does not continue far beneath the observed 2.9 km vertical range of outcrops. Estimates of the volume of granitic material eroded by glaciation based on the glacial till around the pluton concluded that the original uppermost surface of the pluton was unlikely to be much higher than the present summit pinnacles (Sperber 2009). Combining these interpretations suggests that most of the intrusion's original thickness is both exposed and preserved, in agreement with Reinhard & Wenk (1951).

292 *Individual unit volumes*

293 Based on the field data described above, pre-erosional volumetric estimates can be
294 made for each of Mt Kinabalu's composite units (summarised in Table 1 and Fig. 7).

295 Both the upper and lower contacts of the Alexandra Tonalite/Granodiorite were
296 observed in the field, so a good estimate of the unit's thickness can be made (~0.2 km).
297 However it is unclear how much of its lateral extent has been lost to erosion. Equation 1
298 describes the relationship between an intrusion's width and thickness, predicting a
299 lateral unit extent of 0.1 km (0.06-0.3 km within error). The unit has an equivalent circle
300 diameter of 1.3 km, greater than the predicted lateral width, so it is unlikely much
301 material is missing laterally. The unit has an ellipsoidal form in the field (Fig. 7), so
302 modelling it as an ellipsoid with the observed dimensions equates to a total volume of
303 0.2 km^3.

304 The upper and lower contacts of the Low's Granite on the Western Plateau were also
305 observed, so the same methodology can be applied as for the previous unit.
306 Extrapolating the contact surfaces (Fig. 6) predicts a unit thickness of ~0.6 km,
307 corresponding to an intrusion width of 1.1 km (0.7-1.6 km within error) according to
308 Equation 1. The unit's outcrop extent has an equivalent circle diameter of 2.3 km,
309 indicating that little material has been lost laterally. Again modelling the unit as an
310 ellipsoid (Fig. 7) gives a unit volume of ~2 km^3.

311 The extent and structure of the Low's Granite on the northern flank of the pluton (Fig. 3)
312 are highly ambiguous and poorly constrained, although outcrops were observed over a
313 500 m vertical range. Modelling the unit as an ellipsoid and calculating its thickness using
314 Equation 1 predicts a volume of ~3.9 ±0.5 km^3, although this is highly speculative
315 compared to the other units.

316 The King Granite has a more irregular structure than the preceding units of the Western
317 Plateau, and its basal contact is not observed. However, its eastern contact on the
318 Eastern Plateau dips west beneath the intrusion, allowing interpretation of its basal
319 surface (Fig. 6). This estimates a thickness of ~2.3 km, comparable to the 2.2 km
320 predicted by Equation 1. Modelling the unit as an ellipsoid gives a unit volume of ~90
321 km^3.

The Donkey Granite is well constrained in its length and width, and although it was observed 600m below the plateaux in Low's Gully, it is unclear how far it continues at depth. Allowing a further 200 m and modelling the unit as a cuboid sheet (Fig. 7) equates to a volume of 0.4 km^3.

The structure of the Paka Porphyritic Granite is irregular as it intruded around the King Granite (Fig. 7), and the form of its basal contact cannot be predicted. However, although the outcrop width varies from 0.2-1.5 km around the pluton, it is most commonly around 800 m and so we model it here as a sheet (Fig. 6). This is supported by the dip of the outer western contact beneath the pluton (Fig. 3), implying the unit doesn't widen at depth, and the previous calculation that based on Equation 1 most of the pluton's thickness is exposed. Based on these interpretations we predict a unit volume of ~40 km^3.

The basal structure of the Mesilau Porphyritic Granite is again ambiguous and unexposed. Based on the lateral extent of the unit, Equation 1 predicts a thickness of 1.9 km, comparable to the 1.9 km thickness predicted by interpreting a regular basal surface along the pre-emplacement interface of the basement and cover rock (Fig. 6). This is again supported by the previous interpretation based on Equation 1 that the pluton does not continue far at depth. Based on this interpretation of a regular basal surface, the structure of the unit in the field appears to resemble a spherical cap thickening laterally towards its centre (Fig. 6 and 7). Modelling the unit as such predicts a volume of ~40 km^3.

Emplacement conditions

Vogt & Flower (1989) employed an Al-in-hornblende geobarometer to estimate emplacement pressures of 1-3 kbar (equivalent to 3-10 km) for the Alexandra Tonalite/Granodiorite and the Low's and King Granites. This estimation has been improved by combining $^{40}Ar/^{39}Ar$, zircon fission track and (U-Th-Sm)/He thermochronometry to give an upper to mid-crustal emplacement depth of 7-12km (Cottam *et al.* 2013).

Metamorphic temperatures in country rocks can be used to estimate the minimum emplacement temperature of an intrusion. Talc and anthophyllite formed by contact

metamorphism of ultramafic bodies imply temperatures of 630-700°C at emplacement pressures of 2-3 kbar (Bucher & Grapes 2011). Talc is absent from ultramafic samples far from the contact, indicating that these are contact metamorphic phases. The temperature range overlaps the 470-650°C implied by a hornfels containing coexisting muscovite, biotite and cordierite near the intrusive contact (Bucher & Grapes 2011). These temperatures are consistent with low pressure melting experiments (2-3 kbar) indicating a whole rock solidus of ~670-700°C for granitoids of a similar mineralogical and chemical composition to the main granitic units of Mt Kinabalu (Naney 1983, Lambert & Wyllie 1974, Klimm *et al.* 2003, Holtz & Johannes 1994). The presence of hornblende at these temperatures implies high H_2O contents (>5 wt.%; Bogaerts *et al.* 2006).

Accommodation space

Whether melt emplacement was accommodated through roof lifting or floor depression differentiates laccolithic and lopolithic emplacement mechanisms and can be determined from country rock structures. Sedimentary beds >1.9 km to the north, south, southwest and southeast of Mt Kinabalu dip towards the south and/or west (dominantly southwest), reflecting deformation of the Crocker sediments prior to the intrusion of Mt Kinabalu. However, beds closer to the pluton strike sub parallel to the contact and dip away from the pluton. This reorientation of the country rock structures implies that the sedimentary units bow upwards over the pluton (Fig. 6) with accommodation space created through upward deformation and roof lifting of the overlying sediments in a laccolith style, although floor depression may also have occurred (Cruden 1998). Earlier units were also tilted by each subsequent intrusion, producing the westward inclination of the Alexandra Tonalite/Granodiorite and Low's Granite contact surfaces. The intrusion was emplaced at the contact of the basement sedimentary cover rocks, and it was likely this interface that halted magma ascent and determined the depth of emplacement (Clemens & Mawer 1992).

Internal structure and implications for pluton emplacement mechanisms

In current models of composite pluton growth, successive pulses intrude above or below their predecessors as horizontal tabular bodies (Cruden 1998, Cruden 2006, Grocott *et al.* 2009). The exhumation and preservation of peripheral material at Mt Kinabalu

provides a unique opportunity to observe the three dimensional internal structure of a pluton and to test this model of composite pluton growth.

The initial two units have tabular forms suggesting that magma spread laterally upon reaching its emplacement level (Fig. 7); the second (Low's Granite) emplaced below the first (Alexandra Tonalite/Granodiorite). This closely resembles the sheeted laccolith model (Cruden 1998, Cruden 2006, Wiebe & Collins 1998, de Saint-Blanquat *et al.* 2006) as previously advocated for Mt Kinabalu (Cottam *et al.* 2010). However, these early units diverge slightly from the general model as the Low's Granite ascended around the sides of the Alexandra Tonalite/Granodiorite and enveloped its periphery (Fig. 7). Further upward deformation accommodated the King Granite, tilting both the earlier intrusions and their overburden (Fig. 6) in a similar manner to other composite plutons (Stevenson *et al.* 2007, Grocott *et al.* 2009). The King Granite formed a major impediment for the upwelling Paka Porphyritic Granite magma which (unlike the Donkey Granite) was unable able to ascend through the now-crystallised body. Unable to deform or uplift the earlier bodies but still experiencing positive buoyancy, the Paka Porphyritic Granite ascended around the periphery of the earlier units (Fig. 6 and 7) rather than extending laterally at the same crustal level they had exploited. Finally, again restricted by the earlier units, the Mesilau Porphyry intruded beneath the intrusion and extended laterally to the SE (Fig. 7).

Mt Kinabalu highlights the effect of pre-existing granite pseudo-stratigraphy on magma emplacement, producing a complex internal structure (Fig. 7). Instead of the intrusion of each pulse being independent of those before, emplacement was affected by the structure and crystallisation state of the earlier intrusions. At any instant the existing structure controlled the spatial distribution of subsequent intrusions, forcing later pulses in a particular direction with the granite-country rock contacts of earlier units being intruded preferentially over the original emplacement depth of the sediment-ophiolite contact.

Tectonic setting

Dyke and fault orientations were recorded from within the pluton to determine the syn-magmatic tectonic setting and associated paleostresses (Fig. 11), although shear sense

411 indicators were largely lacking. In both compressive and extensional regimes, dykes will
412 propagate perpendicular to the direction of minimum compressive stress (σ3), parallel
413 to the plane containing the maximum (σ1) and intermediate (σ2) compressive stresses
414 (Fig. 12a and 12 c). In contrast, all shear fractures (faults) will propagate obliquely to σ1
415 and in an extensional regime will strike parallel to σ2 (Fig. 12b and 12d; Bles & Feuga
416 1986, Park 1997). Consequently, in extensional regimes (i.e. where σ1 is vertical) faults
417 and dykes will share similar strike orientations, whilst in compressive regimes (i.e. where
418 σ1 is not vertical) the two populations will have different strike orientations (Fig. 12).

419 Measurements from faults and both aplite and intrusive dykes (dominantly pyroxene
420 monzonite) show dominantly steep dips and similar strike orientations trending ENE-
421 WSW (Fig. 11), as would be expected in an extensional regime (Fig. 12a and 12b). A
422 limited number of shear sense indicators were observed but showed no preferred
423 orientation or sense of movement.

424 Although the faults and pyroxene monzonite dykes have not been dated and may
425 significantly post-date intrusion of the Mt Kinabalu pluton, aplite dykes are
426 contemporaneous with the pluton as they are generated from residual, highly
427 fractionated interstitial melts infilling extensional fractures during the crystallisation and
428 contraction of their granitic host (Best 2003). Consequently the steeply NNW-SSE dipping
429 orientation of the aplite dykes indicates a subhorizontal NNW-SSE oriented σ3 direction
430 (Fig. 11). The ENE-WSW strike of the aplite dykes is shared by both the faults and
431 pyroxene monzonite dykes, so the subhorizontal NNW-SSE orientation of σ3 can be
432 interpreted to continue during and after intrusion of the pluton. It should be noted,
433 however, that whilst the fault and pyroxene monzonite dyke orientations are largely
434 concentrated in a common ENE-WSW strike (Fig. 11), the aplite dyke orientations are
435 more dispersed. As aplites are formed during the crystallisation and contraction of their
436 host pluton this is likely the result of localised stresses produced by the contraction being
437 superimposed on the regional stress field. These localised stresses may also explain the
438 more minor dispersed orientations of the faults and pyroxene monzonite dykes.

439 In contrast with the interpretation of the regional stress field from the field data, the
440 intrusion of magma in to the crust can perturb the local stress field during emplacement

(Vigneresse *et al.* 1999). However, the stresses induced by magma emplacement produce fractures and dykes whose strikes radiate from or are concentric around the central point of emplacement induced pressure (likely the core of the pluton or dyke, Castro 1984). The dyke and fault orientations of Mt Kinabalu do not show such a distribution, indicating their formation was influenced by regional stresses not perturbed by local syn-emplacement stresses. Furthermore, any stresses related to magmatic emplacement superimposed on the regional stress field would wane following emplacement, resulting in different interpreted stress directions for the aplite dykes (shortly after emplacement) and faults (later post emplacement) which is not the case (Fig. 11).

These observations indicate NNW-SSE orientated regional extension during emplacement of the pluton (the σ3 direction), supporting previous interpretations (Cottam *et al.* 2013, Hall 2013) that the emplacement and uplift of the pluton was associated with contemporaneous crustal extension. Vogt & Flower (1989) and Swauger *et al.* (2000) ascribed melt generation and uplift to compression and crustal thickening associated with the Sabah Orogeny. However, the revised Late Miocene ages for the emplacement and uplift of the pluton (Cottam *et al.* 2013, Cottam *et al.* 2010) significantly post-date this Early Miocene collisional event (Hutchison 1996, Balaguru & Nichols 2004, Hall *et al.* 2008). Post-orogenic extension affected sediments elsewhere in northern Borneo (Hutchison 2000) and may be associated with Miocene extension of the Sulu Sea basin (Hall 2013), NE of Sabah (Fig. 1). The structural data presented here provides evidence for extension in northern Sabah during the Late Miocene, extending the duration and extent of Miocene extension in Borneo. Further evidence should be sought to determine the extent of Late Miocene extension and to prove that this is not purely local extension, as this conclusion implies that tectonic models interpreting the region as in a compressive regime following the cessation of South China Sea spreading (e.g. King *et al.* 2010, Pubellier & Morley 2013) require revaluation.

Conclusions

The Mt Kinabalu granitic intrusion was emplaced in the upper to middle crust over ~0.8 My in the Late Miocene. The pluton was emplaced in a regional extensional setting, and

steeply NNW-SSE dipping dyke and fault orientations suggest a NNW-SSE oriented regional extension direction challenging tectonic models that predict contemporaneous regional compression. The composite Mt Kinabalu intrusion comprises six major units: the oldest unit being a tonalite/granodiorite, followed by three subsequent sub-equigranular granites and two final porphyritic granites (not quartz monzonite as previously suggested). The changing compositions of these composite units reflect an evolving system of magmatic fractionation and assimilation (Burton-Johnson 2013) which will be discussed in a future paper.

Magma was emplaced along the contact of the ultramafic basement and sedimentary overburden where the contact interface halted upward magma migration and initiated lateral intrusion. Emplacement was accommodated by roof uplift and flexure of the overlying sediments, although floor depression may also have occurred. Successive magmatic units were largely emplaced beneath each other. Each successive pulse tilted earlier units, intruded around them and enveloped their periphery, exploiting the granite-country rock contacts of previous units in preference to the basement-cover rock contact exploited by earlier units. This produced an irregular three dimensional internal structure, deviating somewhat from tabular intrusive emplacement models and providing insight in to the 3D structure of composite intrusive bodies.

Acknowledgements

This study was funded by the Natural Environment Research Council as part of a PhD Research Project. We would like to thank Sandy Cruden and Michel de Saint-Blanquat for their helpful and thorough reviews of our submitted manuscript. In addition we wish to thank Alim Biun, Felix Tongkul and Maklarin Lakim for their assistance in facilitating the field season; Jamili Nais of Sabah Parks who allowed us to work in the National Park; Kate Saunders for her help with the DEM; the mountain guides and researchers of Mt Kinabalu National Park, especially Alijen “Jen”, Halli, Jasirin, Sokaibin, Maklarin Lakim, Sapinus, Samuel and Nicholas; and we thank the SE Asia Research Group at Royal Holloway for their support throughout this project. We also kindly acknowledge Mike Cottam, Christian Sperber and Antony van der Ent for their assistance, discussions and field material.

500 BALAGURU, A. & NICHOLS, G. 2004. Tertiary stratigraphy and basin evolution, southern
501 Sabah (Malaysian Borneo). *Journal of Asian Earth Sciences*, **23**, 537–554, doi:
502 10.1016/j.jseaes.2003.08.001.

503 BALAGURU, A., NICHOLS, G. & HALL, R. 2003. Tertiary stratigraphy and basin evolution of
504 southern Sabah: implications for the tectono-stratigraphic evolution of Sabah,
505 Malaysia. *Bulletin of the Geological Society of Malaysia*, **47**, 27–49.

506 BEST, M.G. 2003. *Igneous and Metamorphic Petrology*. Malden, MA, USA, Blackwell
507 Publishing.

508 BLES, J.L. & FEUGA, B. 1986. *The Fracture of Rocks*. New York, USA, Elsevier Science B.V.

509 BOGAERTS, M., SCAILLET, B. & AUWERA, J.V. 2006. Phase Equilibria of the Lyngdal
510 Granodiorite (Norway): Implications for the Origin of Metaluminous Ferroan
511 Granitoids. *Journal of Petrology*, **47**, 2405–2431, doi: 10.1093/petrology/egl049.

512 BUCHER, K. & GRAPES, R. 2011. *Petrogenesis of Metamorphic Rocks*, 8th Edition.
513 Heidelberg, Germany, Springer.

514 BURTON-JOHNSON, A. 2013. *Origin, Emplacement and Tectonic Relevance of the Mt.*
515 *Kinabalu Granitic Pluton of Sabah, Borneo*. Durham University.
516 http://etheses.dur.ac.uk/9450/.

517 CASTRO, A. 1984. Emplacement fractures in granite plutons (Central Extremadura
518 batholith, Spain). *Geologische Rundschau*, **73**, 869–880.

519 CLEMENS, J.D. & MAWER, C.K. 1992. Granitic magma transport by fracture propagation.
520 *Tectonophysics*, **204**, 339–360, doi: 10.1016/0040-1951(92)90316-X.

521 COLLENETTE, P. 1958. *The Geology and Mineral Resources of the Jessleton-Kinabalu Area,*
522 *North Borneo*. Kuching, Srawak, Geological Survey Department, British Territories
523 in Borneo.

524 COLLENETTE, P. 1965. The geology and mineral resources of the Pensiangan and Upper
525 Kinabatangan area, Sabah. *Malaysia Geological Survey Borneo Region, Memoir*
526 *12*, 150.

527 COTTAM, M.A., HALL, R., SPERBER, C. & ARMSTRONG, R. 2010. Pulsed emplacement of the
528 Mount Kinabalu granite, northern Borneo. *Journal of the Geological Society*, **167**,
529 49–60, doi: 10.1144/0016-76492009-028.Pulsed.

530 COTTAM, M.A., HALL, R., SPERBER, C., KOHN, B.P., FORSTER, M.A. & BATT, G.E. 2013. Neogene
531 rock uplift and erosion in northern Borneo: evidence from the Kinabalu granite,
532 Mount Kinabalu. *Journal of the Geological Society*, **170**, 805–816, doi:
533 10.1144/jgs2011-130.

534 CRUDEN, A.R. 1998. On the emplacement of tabular granites. *Journal of the Geological*
535 *Society*, **155**, 853–862.

536 CRUDEN, A.R. 2006. Emplacement and growth of plutons: implications for rates of melting
537 and mass transfer in continental crust. *In*: *Evolution and Differentiation of the*
538 *Continental Crust*. Cambridge, UK, Cambridge University Press.

539 CRUDEN, A.R. & MCCAFFREY, K.J.W. 2001. Growth of plutons by floor subsidence:
540 implications for rates of emplacement, intrusion spacing and melt-extraction
541 mechanisms. *Physics and Chemistry of the Earth, Part A: Solid Earth and Geodesy*,
542 **26**, 303–315, doi: 10.1016/S1464-1895(01)00060-6.

543 CULLEN, A.B. 2010. Transverse segmentation of the Baram-Balabac Basin, NW Borneo:
544 refining the model of Borneo's tectonic evolution. *Petroleum Geoscience*, **16**, 3–
545 29, doi: 10.1144/1354-079309-828.

546 DE SAINT-BLANQUAT, M., LAW, R.D., BOUCHEZ, J.-L. & MORGAN, S.S. 2001. Internal structure
547 and emplacement of the Papoose Flat pluton: An integrated structural,
548 petrographic, and magnetic susceptibility study. *Geological Society of America*
549 *Bulletin*, **113**, 976–995.

550 DE SAINT-BLANQUAT, M., HABERT, G., HORSMAN, E., MORGAN, S.S., TIKOFF, B., LAUNEAU, P. &
551 GLEIZES, G. 2006. Mechanisms and duration of non-tectonically assisted magma
552 emplacement in the upper crust: the Black Mesa pluton, Henry Mountains, Utah.
553 *Tectonophysics*, **428**, 1–31.

554 DE SILVA, S.L. & GOSNOLD, W.D. 2007. Episodic construction of batholiths: insights from the
555 spatiotemporal development of an ignimbrite flare-up. *Journal of Volcanology*
556 *and Geothermal Research*, **167**, 320–335.

557 DHONAU, T.J. & HUTCHISON, C.S. 1965. The Darvel Bay area, East Sabah, Malaysia. *Malaysia*
558 *Geological Survey Borneo Region, Annual Report for 1965*, 141–160.

559 GROCOTT, J., ARÉVALO, C., WELKNER, D. & CRUDEN, A.R. 2009. Fault-assisted vertical pluton
560 growth: Coastal Cordillera, north Chilean Andes. *Journal of the Geological Society*,
561 **166**, 295–301.

562 HALL, R. 1996. Reconstructing Cenozoic SE Asia. *In*: Hall, R. & Blundell, D. J. (eds) *Tectonic*
563 *Evolution of SE Asia*. Geological Society, London, Special Publications, **106**, 153–
564 184.

565 HALL, R. 2013. Contraction and extension in northern Borneo driven by subduction
566 rollback. *Journal of Asian Earth Sciences*, **76**, 399–411, doi:
567 10.1016/j.jseaes.2013.04.010.

568 HALL, R. & WILSON, M.E.J. 2000. Neogene sutures in eastern Indonesia. *Journal of Asian*
569 *Earth Sciences*, **18**, 781–808.

570 HALL, R., VAN HATTUM, M.W. A. & SPAKMAN, W. 2008. Impact of India–Asia collision on SE
571 Asia: The record in Borneo. *Tectonophysics*, **451**, 366–389, doi:
572 10.1016/j.tecto.2007.11.058.

573 HAZEBROEK, H.P. & TAN, D.N.K. 1993. Tertiary tectonic evolution of the NW Sabah
574 continental margin. *Bulletin of the Geological Society of Malaysia*, **33**, 195–210.

575 HOLTZ, F. & JOHANNES, W. 1994. Maximum and minimum water contents of granitic melts:
576 implications for chemical and physical properties of ascending magmas. *Lithos*,
577 **32**, 149–159.

578 HORSMAN, E., MORGAN, S., DE SAINT-BLANQUAT, M., HABERT, G., NUGENT, A., HUNTER, R.A. &
579 TIKOFF, B. 2009. Emplacement and assembly of shallow intrusions from multiple
580 magma pulses, Henry Mountains, Utah. *Earth and Environmental Science*
581 *Transactions of the Royal Society of Edinburgh*, **100**, 117–132.

582 HUTCHISON, C. 1978. Ophiolite metamorphism in northeast Borneo. *Lithos*, 195–208.

583 HUTCHISON, C. 2000. A Miocene collisional belt in north Borneo: uplift mechanism and
584 isostatic adjustment quantified by thermochronology. *Journal of the Geological*
585 *Society*, **157**, 783–793.

586 HUTCHISON, C.S. 1996. The 'Rajang accretionary prism' and 'Lupar Line' problem of
587 Borneo. *Geological Society, London, Special Publications*, **106**, 247–261, doi:
588 10.1144/GSL.SP.1996.106.01.16.

589 HUTCHISON, C.S. 2005. *Geology of North-West Borneo: Sarawak, Brunei and Sabah*.
590 Elsevier.

591 IMAI, A. & OZAWA, K. 1991. Tectonic implications of the hydrated garnet peridotites near
592 Mt Kinabalu, Sabah, East Malaysia. *Journal of Southeast Asian Earth Sciences*, **6**,
593 431–445.

594 JACOBSON, G. 1970. *Gunung Kinabalu Area, Sabah, Malaysia*. Kuching, Sarawak, Geological
595 Survey Malaysia.

596 KASAMA, T., AKIMOTO, H., HADA, S. & JACOBSON, G. 1970. Geology of the Mt. Kinabalu area,
597 Sabah, Malaysia. *Journal of Geosciences, Osaka City University*, **13**, 113–148.

598 KING, R.C., BACKÉ, G., MORLEY, C.K., HILLIS, R.R. & TINGAY, M.R.P. 2010. Balancing
599 deformation in NW Borneo: Quantifying plate-scale vs. gravitational tectonics in
600 a delta and deepwater fold-thrust belt system. *Marine and Petroleum Geology*,
601 **27**, 238–246, doi: 10.1016/j.marpetgeo.2009.07.008.

602 KIRK, H.J.C. 1968. *The Igneous Rocks of Sarawak and Sabah*. US Government Printing
603 Office.

604 KLIMM, K., HOLTZ, F., JOHANNES, W. & KING, P.L. 2003. Fractionation of metaluminous A-type
605 granites: an experimental study of the Wangrah Suite, Lachlan Fold Belt,
606 Australia. *Precambrian Research*, **124**, 327–341.

KOOPMANS, B.N. 1967. Deformation of the metamorphic rocks and the Chert–Spilite Formation in the southern part of the Darvel Bay area, Sabah. *Geological Survey of Malaysia, Borneo Region, Bulletin*, **8**, 14–24.

LAMBERT, I.B. & WYLLIE, P.J. 1974. Melting of tonalite and crystallization of andesite liquid with excess water to 30 kilobars. *The Journal of Geology*, 88–97.

LEONG, K.M. 1974. *The Geology and Mineral Resources of the Upper Segama Valley and Darvel Bay Area, Sabah, Malaysia*. US Government Printing Office.

MCCAFFREY, K.J.W. & PETFORD, N. 1997. Are granitic intrusions scale invariant? *Journal of the Geological Society*, **154**, 1–4, doi: 10.1144/gsjgs.154.1.0001.

MORLEY, C.K. & BACK, S. 2008. Estimating hinterland exhumation from late orogenic basin volume, NW Borneo. *Journal of the Geological Society*, **165**, 353–366.

NANEY, M. 1983. Phase equilibria of rock-forming ferromagnesian silicates in granitic systems. *American Journal of Science*.

NEWTON-SMITH, J. 1967. *Bidu-Bidu Hills Area: Sabah, East Malaysia*. Geological Survey, Geological Survey of Malaysia, Borneo Region, Bulletin 4.

NOAD, J.J. 1998. *The Sedimentary Evolution of the Tertiary of Eastern Sabah, Northern Borneo.* PhD Thesis, Birkbeck, University of London.

OMANG, S. A. K. & BARBER, A. J. 1996. Origin and tectonic significance of the metamorphic rocks associated with the Darvel Bay Ophiolite, Sabah, Malaysia. *Geological Society, London, Special Publications*, **106**, 263–279, doi: 10.1144/GSL.SP.1996.106.01.17.

PARK, R.G. 1997. *Foundations of Structural Geology*. London, UK, Routledge.

PETFORD, N. & CLEMENS, J. 2000. Granites are not diapiric! *Geology Today*, 180–184.

PETFORD, N., CRUDEN, A.R., MCCAFFREY, K.J. & VIGNERESSE, J.L. 2000. Granite magma formation, transport and emplacement in the Earth's crust. *Nature*, **408**, 669–673, doi: 10.1038/35047000.

PUBELLIER, M. & MORLEY, C.K. 2013. The Basins of Sundaland (SE Asia); evolution and boundary conditions. *Marine and Petroleum Geology*.

RANGIN, C. & SILVER, E.A. 1990. Geological setting of the Celebes and Sulu Seas. *In*: Silver, E. A., Rangin, C. & von Breymann, M. T. (eds) *Proceedings of the Ocean Drilling Program, Initial Reports 124*. 35–42.

REINHARD, M. & WENK, E. 1951. Geology of the Colony of North Borneo. *British Borneo Geological Survey Bulletin*, **1**.

SANDAL, S.T. (ed.). 1996. *The Geology and Hydrocarbon Resources of Negara Brunei Darussalem*. Brunei Museum, Syabas Bandar Seri Begawan, Brunei Darussalem.

642 SPERBER, C. 2009. *The Thermotectonic Development of Mount Kinabalu, Sabah, Malaysia:*
643 *Constraints from Low-Temperature Thermochronology*. PhD Thesis, Royal
644 Holloway, University of London.

645 STEVENSON, C.T.E., OWENS, W.H., HUTTON, D.H.W., HOOD, D.N. & MEIGHAN, I.G. 2007.
646 Laccolithic, as opposed to cauldron subsidence, emplacement of the Eastern
647 Mourne pluton, N. Ireland: evidence from anisotropy of magnetic susceptibility.
648 *Journal of the Geological Society*, **164**, 99–110, doi: 10.1144/0016076492006-
649 008.

650 SWAUGER, D.A., HUTCHISON, C.S., BERGMAN, S.C. & GRAVES, J.E. 2000. Age and emplacement
651 of the Mount Kinabalu pluton. *Geological Society of Malaysia Bulletin*, **44**, 159–
652 163.

653 TAYLOR, B. & HAYES, D.E. 1983. Origin and history of the South China Sea basin. *In*: Hayes,
654 D. E. (ed.) *The Tectonic and Geologic Evolution of Southeast Asian Seas and*
655 *Islands: Part 2*. American Geophysical Union, Geophysical Monographs Series, **27**,
656 23–56.

657 TONGKUL, F. 1991. Tectonic evolution of Sabah, Malaysia. *Journal of Southeast Asian Earth*
658 *Sciences*, **6**, 395–405.

659 TONGKUL, F. 1994. The geology of Northern Sabah, Malaysia: its relationship to the
660 opening of the South China Sea Basin. *Tectonophysics*, **235**, 131–147.

661 TONGKUL, F. & CHANG, F.K. 2003. Structural geology of the Neogene Maliau Basin, Sabah.
662 *Bulletin of the Geological Society of Malaysia*, **47**, 51–61.

663 VAN HATTUM, M.W., HALL, R., PICKARD, A.L. & NICHOLS, G.J. 2006. Southeast Asian sediments
664 not from Asia: Provenance and geochronology of north Borneo sandstones.
665 *Geology*, **34**, 589–592.

666 VIGNERESSE, J.L. 2006. Granitic batholiths: from pervasive and continuous melting in the
667 lower crust to discontinuous and spaced plutonism in the upper crust.
668 *Transactions of the Royal Society of Edinburgh: Earth Sciences*, **97**, 311–324.

669 VIGNERESSE, J.L. & CLEMENS, J.D. 2000. Granitic magma ascent and emplacement: neither
670 diapirism nor neutral buoyancy. *Geological Society, London, Special Publications*,
671 **174**, 1–19, doi: 10.1144/GSL.SP.1999.174.01.01.

672 VIGNERESSE, J.-L., TIKOFF, B. & AMÉGLIO, L. 1999. Modification of the regional stress field by
673 magma intrusion and formation of tabular granitic plutons. *Tectonophysics*, **302**,
674 203–224.

675 VOGT, E. & FLOWER, M. 1989. Genesis of the Kinabalu (Sabah) granitoid at a subduction-
676 collision junction. *Contributions to Mineralogy and Petrology*, 493–509.

677 VOLLMER, F.W. 2015. Orient 3: a new integrated software program for orientation data
678 analysis, kinematic analysis, spherical projections, and Schmidt plots. *In*:
679 *Geological Society of America Abstracts with Programs*. 0.

680 WHITNEY, D.L. & EVANS, B.W. 2010. Abbreviations for names of rock-forming minerals.
681 *American mineralogist*, **95**, 185.

682 WIEBE, R.A. 1988. Structural and magmatic evolution of a magma chamber: the Newark
683 Island layered intrusion, Nain, Labrador. *Journal of Petrology*, **29**, 383–411.

684 WIEBE, R.A. & COLLINS, W.J. 1998. Depositional features and stratigraphic sections in
685 granitic plutons: implications for the emplacement and crystallization of granitic
686 magma. *Journal of Structural Geology*, **20**, 1273–1289.

687

Unit	Alexandra Tn/Gd	Low's Gt	King Gt	Donkey Gt	Paka Pph	Mesilau Pph
U-Pb Age (Ma)	7.85 ±0.08	7.69 ±0.07 – 7.64 ±0.11	7.46 ±0.08 – 7.44 ±0.09	7.46 > t > 7.32	7.32 ±0.09 – 7.22 ±0.07	–
Approx. Vol. (Km^3)	0.2	2 (W) 4 (N)	90	0.4	40	40
Phases (Modal %)						
Qz	23-28	16-28	14-27	23	15-21	7-21
Pl	40-45	25-33	21-38	26	23-33	24-28
Kfs	4-7	18-29	26-36	25	23-35	38-48
Hbl	4-13	21-28	9-21	11	11-24	8-23
Bt	9-19	4-7	0-5	13	1-2	0-5
Cpx	–	–	–	–	–	0-2
Accessory	Ap, Ep	Ap, Ep, Zrn	Ap, Ep, Zrn	Ap	Ap	Ap, Spn

Table 1. Summary of U-Pb zircon ages, estimated volumes and modal mineralogies of the major granitoid units. Abbreviations used: Tn – Tonalite; Gd – Granodiorite; Gt – Granite; Pph – Porphyritic Granite; Qz – Quartz; Pl – Plagioclase; Kfs – Potassium Feldspar; Hbl – Hornblende; Bt – Biotite; Cpx. – Clinopyroxene; Ap – Apatite; Ep – Epidote; Zrn – Zircon; Spn – Sphene (Whitney & Evans 2010).

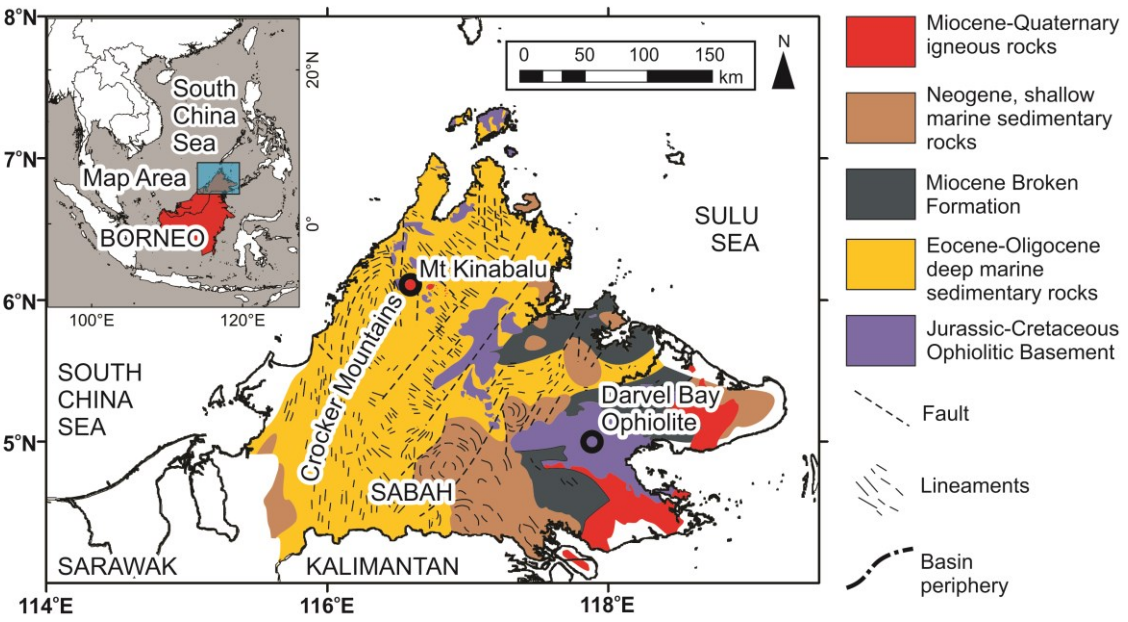

695

696

697 Fig. 1. Simplified geological map of Sabah, adapted from (Kirk 1968), (Balaguru & Nichols
698 2004) and (Hutchison 2005).

699

700 

701

702 Fig. 2. Photo of Mt Kinabalu looking north from the town of Kundasang, 10 km south and
703 2800 m below the summit, illustrating the scale, relief and contrast of the forested lower
704 flanks and glaciated summit plateaux of the mountain.

705

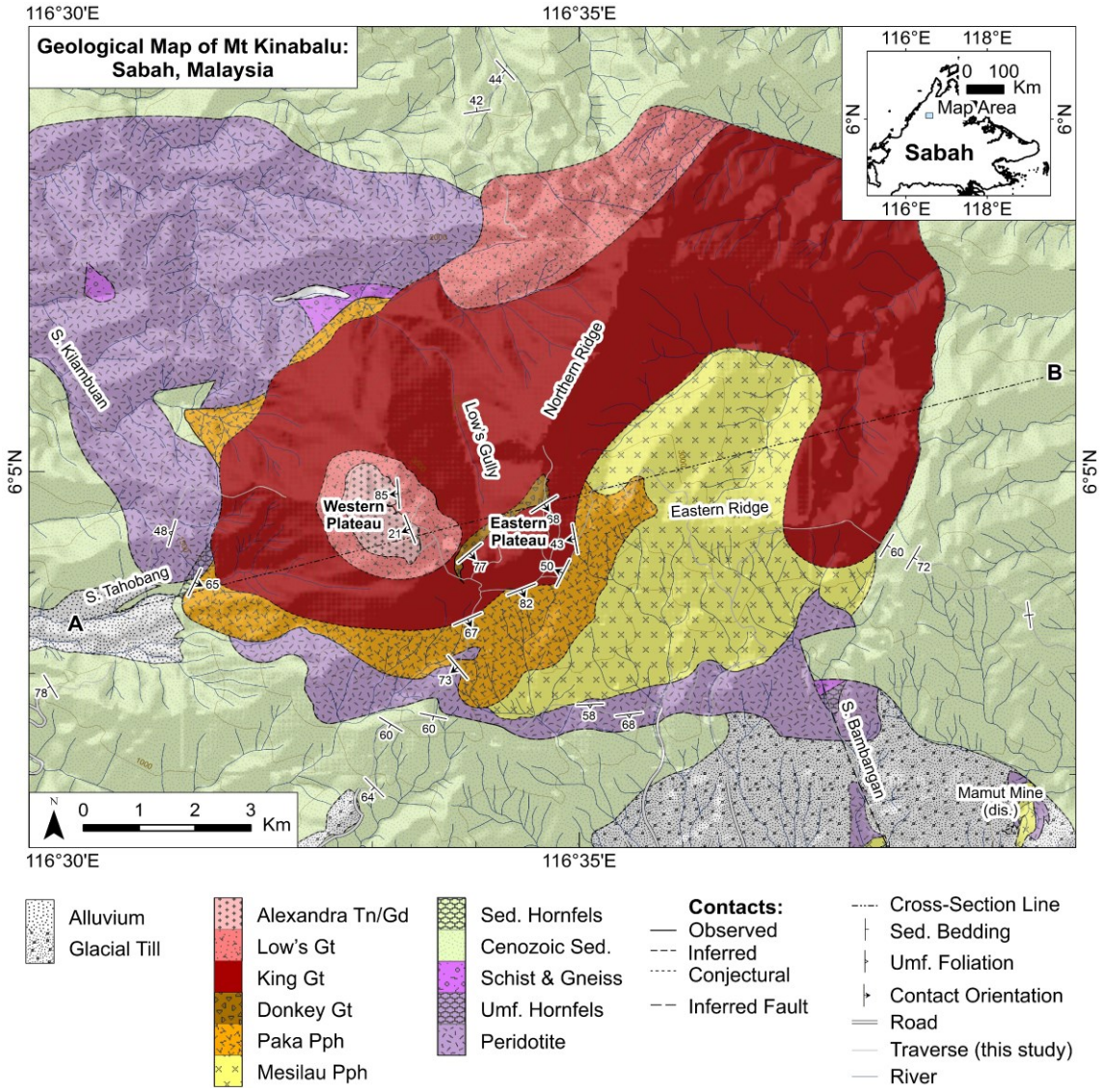

706

707

708 Fig. 3. Geological Map of Mt Kinabalu, combining observations of this study with the
709 map of Jacobson (1970). Inset shows regional geography and study area. Abbreviations
710 used: "S." prefix denotes "Sungai", Malay for "River"; Tn – Tonalite; Gd – Granodiorite;
711 Gt – Granite; Pph – Porphyritic Granite; Sed. – Sedimentary; Umf. – Ultramafic.

712

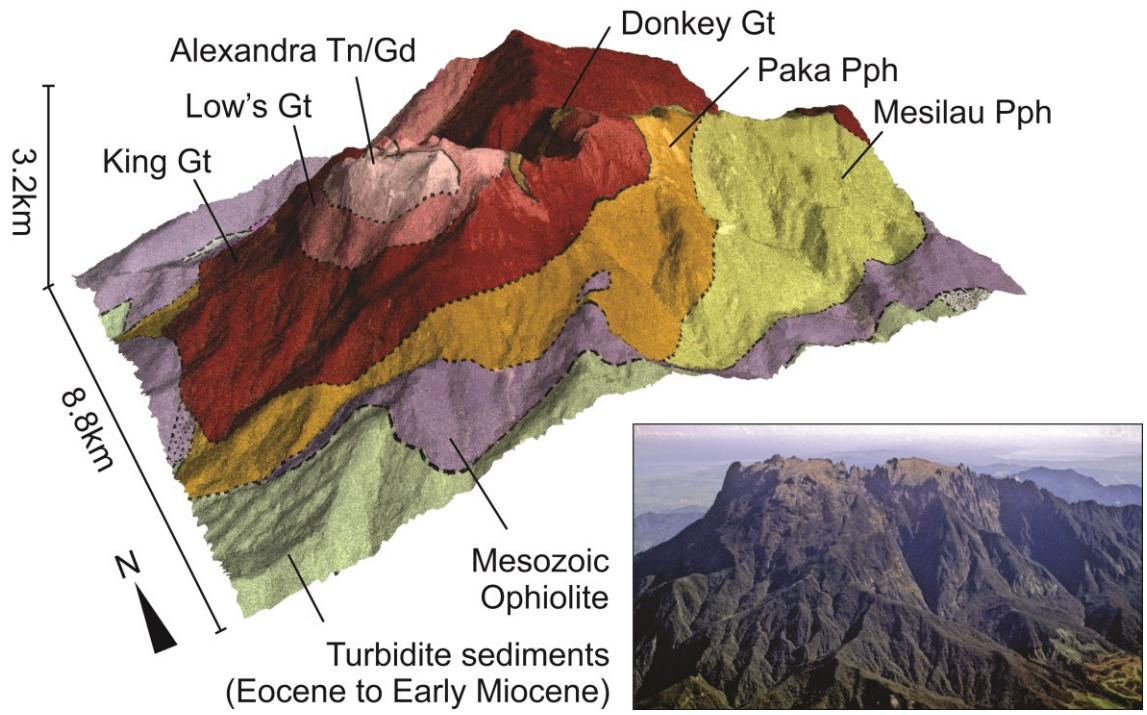

713

714

715 Fig. 4. New geological map overlain on the DEM of the mountain and photo from the air
716 of a similar view for comparison (photo courtesy of Dr Tony Barber, SEARG).
717 Abbreviations as in Fig. 3. Ages of granitic units from Cottam et al. (2010).

718

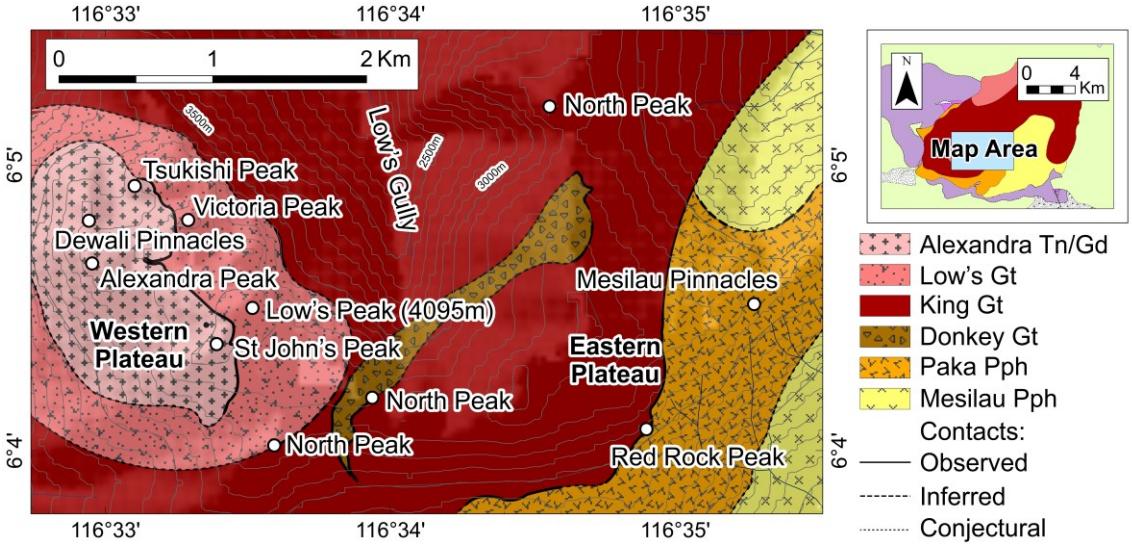

719

720

721 Fig. 5. Summit map of the Western and Eastern plateaux of Mt Kinabalu, separated by
722 Low's Gully, showing the geological interpretation and peak names referred to in the
723 text. Abbreviations as in Fig. 3.

724

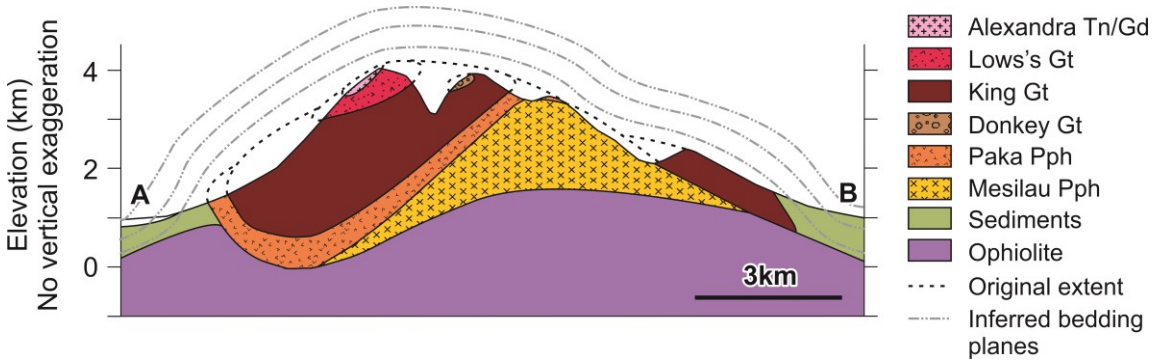

725

726

727 Fig. 6. Interpreted geological cross-sections of the mountain showing the internal
728 structure of the pluton and extrapolated original extent. Line of section as shown in Fig.
729 3. No vertical exaggeration.

730

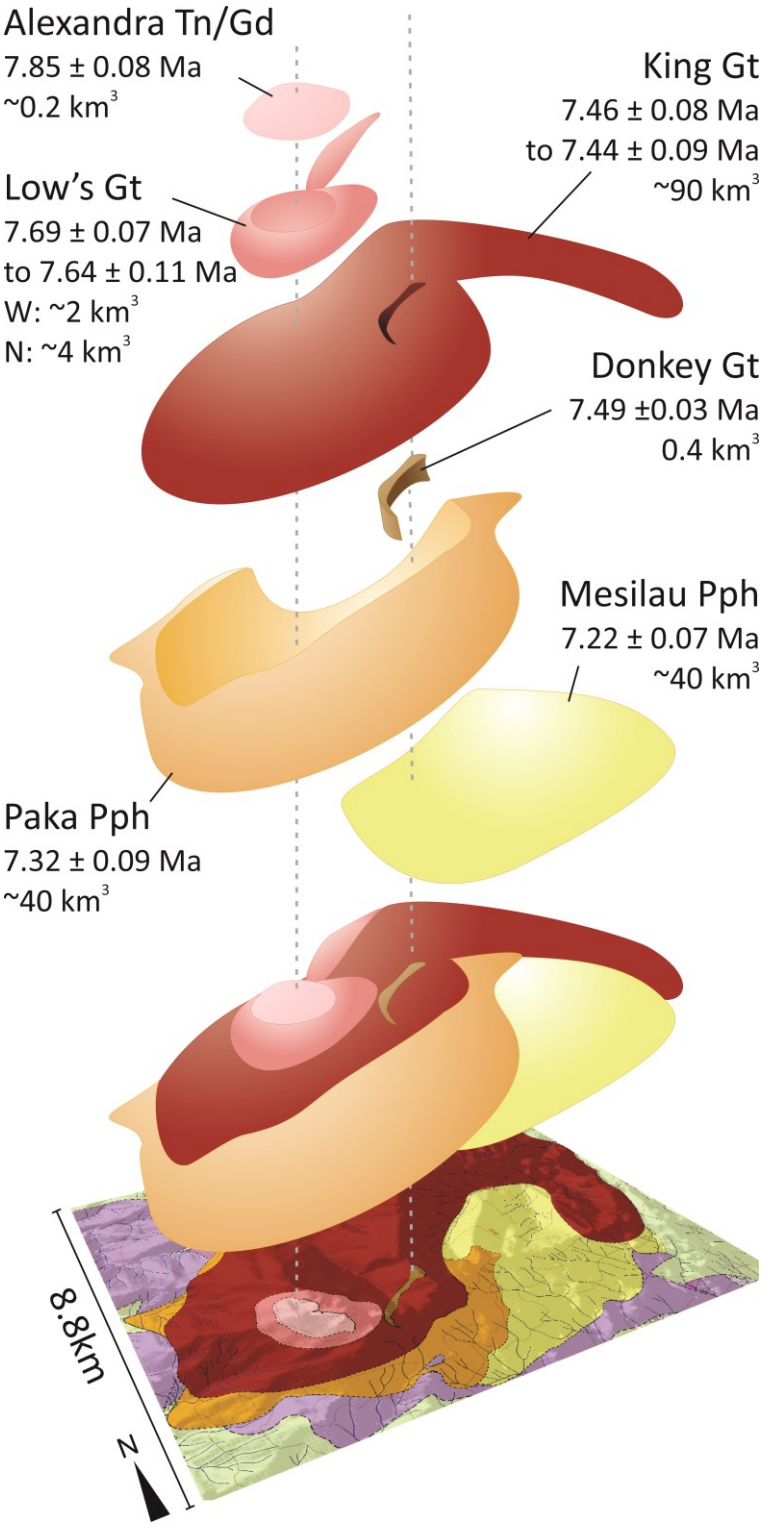

731

732 Fig. 7. Exploded view illustration of the pre-erosional structure of the Mt Kinabalu pluton
733 and its composite units. Emplacement ages from Cottam et al. (2010).Calculated volumes
734 from Table 1. Abbreviations as in Fig. 3.

735

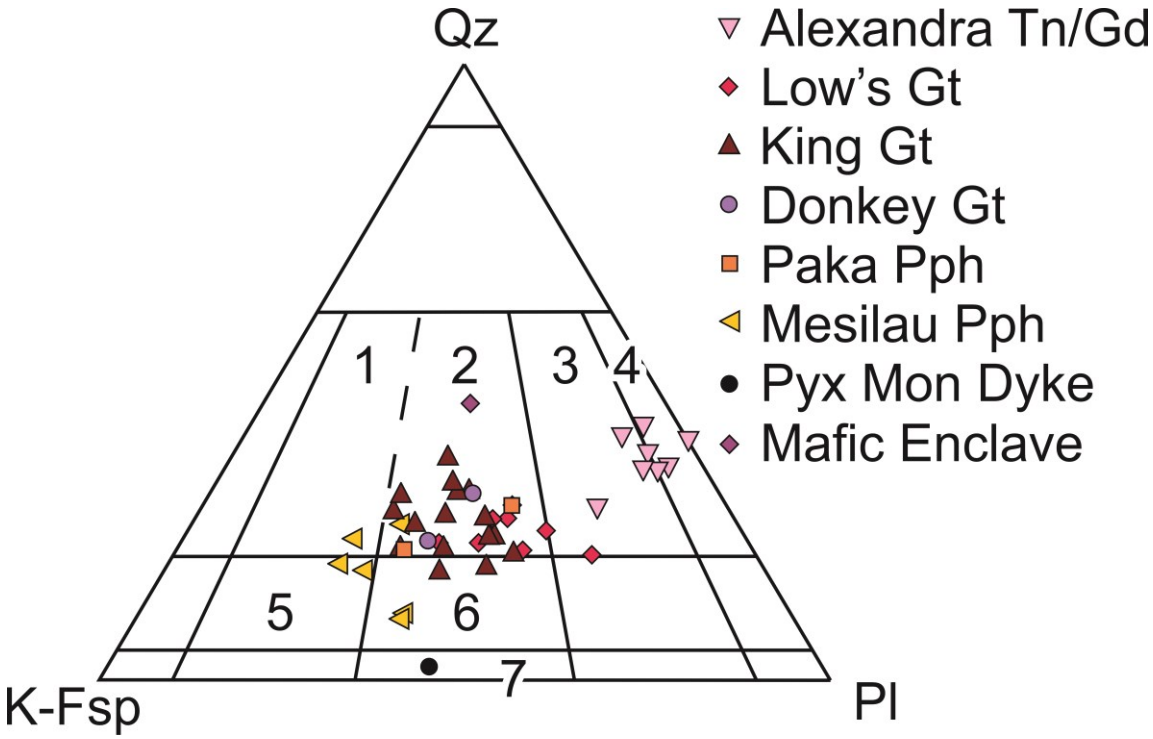

736

737

738 Fig. 8. Classification of the Mt Kinabalu granitoids, according to the modal IUGS-
739 Streckeisen classification (Streckeisen, 1976). Classification codes: (1) Syenogranite; (2)
740 Monzogranite; (3) Granodiorite; (4) Tonalite; (5) Quartz-Syenite; (6) Quartz- Monzonite);
741 (7) Monzonite. Abbreviations as in Fig. 3, plus: Pyx Mon – Pyroxene Monzonite.

742

743

744

745 Fig. 9. View of the Western Plateau looking east, showing the contact between the
746 Alexandra Tonalite/Granodiorite (Alexandra Tn/Gd, foreground) and the Low's Granite
747 (Low's Gt). Field of view ~1.3km;

748

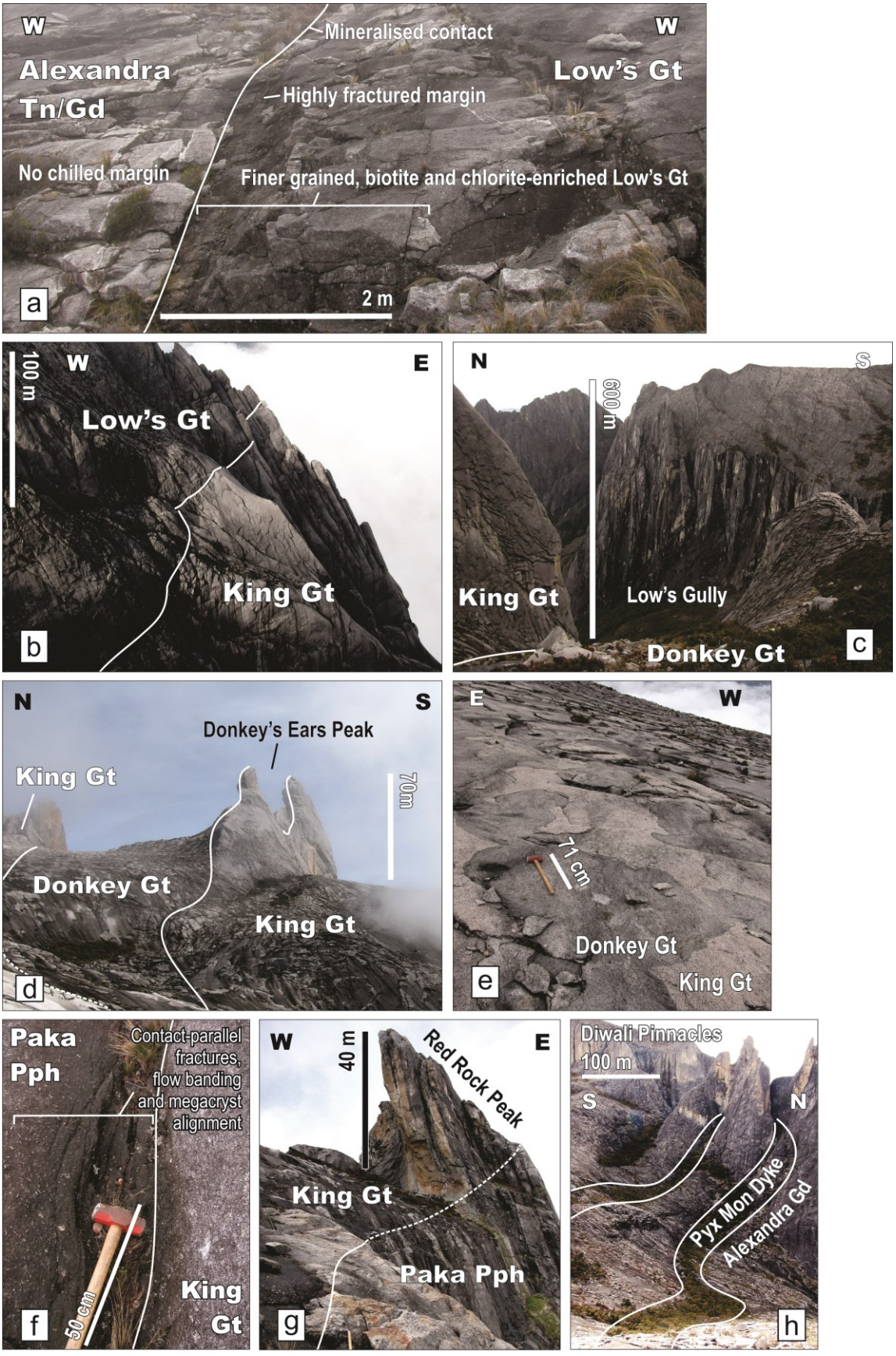
W
Mineralised contact
W
Alexandra Tn/Gd
Low's Gt
Highly fractured margin
No chilled margin
Finer grained, biotite and chlorite-enriched Low's Gt
a
2 m
100 m
W
E
Low's Gt
King Gt
b
N
S
600 m
King Gt
Low's Gully
Donkey Gt
c
N
S
Donkey's Ears Peak
King Gt
70m
Donkey Gt
King Gt
d
E
W
71 cm
Donkey Gt
King Gt
e
Paka Pph
Contact-parallel fractures, flow banding and megacryst alignment
50 cm
King Gt
f
W
40 m
Red Rock Peak
E
King Gt
Paka Pph
g
Diwali Pinnacles
100 m
S
N
Pyx Mon Dyke
Alexandra Gd
h

749

750

Fig. 10. (a) Contact of the Alexandra Tonalite/Granodiorite (Alexandra Tn/Gd) and the Low's Granite (Low's Gt) on the Western Plateau, west of Victoria Peak (Fig. 5). Photo looking north; (b) Contact of the Low's Granite and King Granite (King Gt) units on the eastern cliffs of the Western Plateau. Photo looking north. Field of view ~300 m; (c) Looking east towards Low's Gully from the Donkey Granite outcrops of the Western Plateau, north of the Donkey's Ears (Fig. 5); (d) Contact of the Donkey Granite (Donkey Gt) within the King Granite on the Western Plateau showing the resulting topographic feature of the Donkey's Ears Peak. Photo looking NE from the summit trail; (e) Magma mingling between The Donkey Granite (dark grey unit) and the King Granite (light grey unit) on the NW contact on the Western Plateau. Photo looking south. Sledgehammer for scale; (f) Contact of the King Granite and Paka Porphyritic Granite (Paka Pph) on the southern flanks of Mt Kinabalu where the contact dips steeply south beneath the Paka Porphyritic Granite. Photo looking west; (g) Contact between the King Granite and Paka Porphyritic Granite on the east of the Eastern Plateau showing the Paka Porphyritic Granite dipping beneath the King Granite. Photo looking north. (h) Pyroxene monzonite (Pyx Mon) dykes intruding the Alexandra Tonalite Granodiorite on the north end of the Western Plateau, showing their preferential erosion and vegetation. Photo looking west. Note: Photographs taken in 2011, prior to the damage to the Donkey's Ears Peak during the earthquake of 2015.

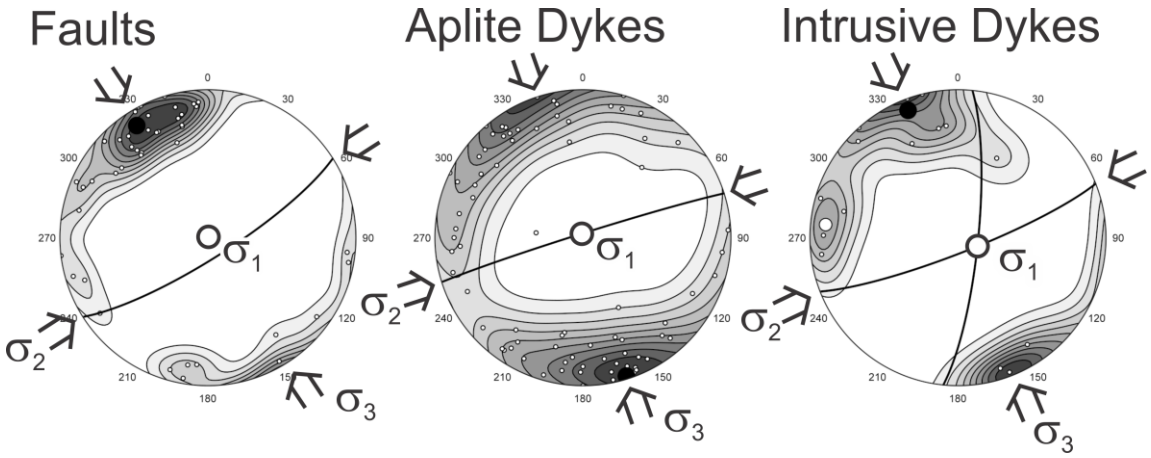

771

772

773 Fig. 11. Stereonets of poles to planes for fault (n = 46), aplite dyke (n = 77) and intrusive
774 dyke (n = 15) orientations on Mt Kinabalu with probability density contours at 10% intervals
775 (Vollmer 2015). The maximum eigenvectors and their great circles are shown (black circles
776 and thick black lines), as are the interpreted principal stress directions. The intrusive dyke
777 orientations are bimodal and the maximum eigenvectors are shown for each domain
778 (black and white circles with corresponding great circles).

779

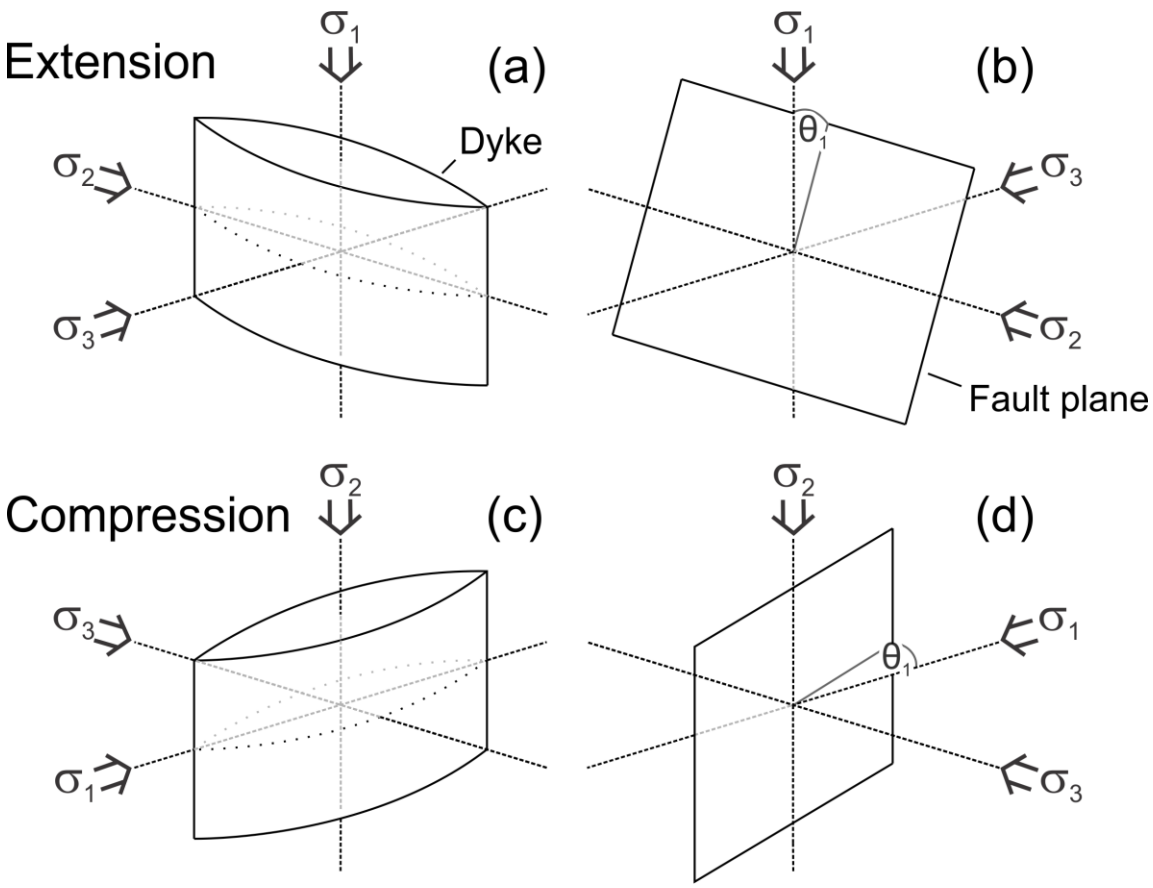

780

781

782 Fig. 12. Illustrations of the relationships between planar dyke (a and c) and fault (b and
783 d) orientations relative to the principal stress axes in compressional and extensional
784 regimes. σ_1 – Maximum compressive stress; σ_2 – Intermediate compressive stress; σ_3 –
785 Minimum compressive stress; θ_1 – Angle between the fault plane and the σ1 axis.